applied sciences

MDPI

Article

Joint Optimization of Voyage and Speed for Semi-Submersible Ships Considering Loading Safety of Heavy Cargo

Ruihao Zhao [1,2], Ruijia Zhao [1,*] and Xianqi Chen [1]

[1] Integrated Transport Institute, Dalian Maritime University, Dalian 116026, China; zhaoruihao2023@126.com (R.Z.); chenxianqi2001@126.com (X.C.)
[2] Merchant Marine College, Shanghai Maritime University, Shanghai 201306, China
* Correspondence: zhaoruijia@dlmu.edu.cn

Abstract

To address the joint optimization problem of heavy-lift cargo stowage and speed decisions during transportation by semi-submersible ships, a joint optimization model of voyage and speed is established for semi-submersible ships. In this model, the initial metacentric height (GM) after free-surface correction is taken as the core safety constraint. Factors such as cargo mass, loading and unloading time windows, ship deadweight, and speed range are comprehensively considered. The objective function is set to minimize total transportation cost. A two-stage method is used to solve the model. Case study results show that the optimized total cost is 20.7% lower than that of the cargo allocation and speed scheme formulated based on manual experience. Fuel cost is reduced by 29.5%. Charter cost and port cost are reduced by 3.1% and 14.3%, respectively. The sensitivity analysis results for the minimum limit of GM and the fuel oil price show that improving the safety standard reduces the compliance of small vessels for heavy-lift cargo. This causes the tight capacity of large vessels. It may even make some cargo transportation demand difficult to satisfy. A rise in the fuel oil price significantly increases the fuel cost and reduces the enterprise profitability. Appropriately reducing speed is an effective strategy to mitigate the effect of the fuel oil price.

Keywords: operational safety; semi-submersible ship; heavy cargo allocation; speed optimization; initial metacentric height

1. Introduction

Maritime transportation is one of the most important modes in international cargo trade. It has advantages such as large transport volume and low freight rates. It has become an important support for global trade [1,2]. Global offshore resource development strategies continue to advance. Cross-regional transportation demand for heavy-lift cargo continues to grow. This cargo includes drilling platforms, oil and gas production equipment, and offshore wind power equipment. Semi-submersible ships have advantages such as adjustable draft, large deck load-bearing area, and navigation stability. They have become one of the main ship types for maritime transportation of heavy-lift cargo [3,4]. However, semi-submersible ship transportation has common characteristics of tramp ships. These characteristics include no fixed routes or schedules, scattered cargo sources, and a high ballast rate. It also has special attributes. These attributes include a large unit cargo mass, strong integrity, and high loading and unloading operation risk. Its operation process must balance safety assurance and cost control. Unbalanced cargo mass distribution can easily cause abnormal

Check for updates

Academic Editor: José A. Orosa García

Received: 28 September 2026
Revised: 14 October 2026
Accepted: 20 October 2026
Published: 4 November 2026

Copyright: © 2026 by the authors. Licensee MDPI, Basel, Switzerland. This article is an open access article distributed under the terms and conditions of the Creative Commons Attribution (CC BY) license.

GM values. This may lead to an excessive rolling amplitude and even capsizing accidents [5]. This weakens the economic benefits of enterprises. Therefore, joint optimization of safety and economy for heavy-lift cargo transportation by semi-submersible ships has become a problem in the interdisciplinary field of ship engineering and shipping management.

In terms of voyage and cargo allocation, Homsi et al. [6] studied actual-scale tramp ship and industrial shipping cases. They used exact solution methods. The results show that cargo selection, time windows, and ship suitability jointly affect the formulation of voyage plans or route plans. In deep-sea cargo transportation scheduling research, scholars incorporated heterogeneous fleets, cargo volume, and time windows into the same model [7]. Considering the uncertainty of the arrival time and quantity of multiple batches of cargo sources, Wu et al. [8] constructed a robust joint optimization model of cargo allocation and route planning. This model simultaneously formulates cargo allocation decisions and route decisions. Recent studies further incorporated tidal berth windows [9] and refueling port selection [10] into the model. Omholt-Jensen et al. [11] studied stochastic decisions of refueling and fleet repositioning. Tamburini et al. [12] combined spot cargo sources, chartering, refueling, and speed in the same framework. These results provide a methodological basis for ship–cargo matching and voyage scheduling under complex constraints. However, their cargo suitability conditions are usually expressed by capacity, port, or operational rules. They pay little attention to stability changes after loading heavy-lift cargo on semi-submersible ships.

In terms of speed decision and voyage planning, reducing speed usually helps control the fuel cost. But it changes the cargo delivery time, subsequent tasks that the ship can undertake, and charter occupation time. Load-related fuel consumption research shows that the ship loading condition affects the relationship between speed and cost [13]. Time-related supply vessel routing research [14] and tramp ship research under uncertain cargo sources [15] reveal that after navigation environment and arrival time change, the original speed and route combination may no longer be optimal. For multi-objective operation, Huang et al. [16] established an ETE-SRSP model. This model balances transport efficiency and emissions. Under carbon intensity (CII) constraints, some scholars considered a joint model of cargo selection and speed [17] and an economic revenue speed model [18]. Learning-based joint optimization of the route and speed has been studied. Weather uncertainty research has also extended speed decisions under complex sea conditions [19–21]. For semi-submersible ships, laden and ballast legs, cargo delivery windows, and subsequent voyages interact with each other. This requires speed configuration by leg. It does not require a single preset speed for the whole ship.

The initial metacentric height of a ship is affected by cargo center of gravity, ballast water distribution, and free-surface effect. Ok et al. [22] linearized the stability constraints of container ships. They incorporated ballast and stability conditions into a computable stowage model. Wang et al. [23] used a neural network method to predict GM in real time. Song et al. [24] studied maneuverability under different GM states. These studies emphasize the role of stability indicators from state estimation and motion response perspectives. Three-dimensional stowage multi-objective optimization [25] and related reviews [26] systematically discussed structural and stability constraints. Multi-port stowage research [27] jointly considered stability requirements and loading and unloading efficiency. Joint optimization of bulk cargo port berths and ballast water [28], risk assessment of ballasting and de-ballasting operations [29], joint optimization of the floating crane lifting trajectory and ballast [30], and de-ballasting scheduling at coal export terminals [31] further show that the ballast condition determines operation feasibility. It also affects the operation time and resource arrangement. However, these results mostly study stowage or in-port operations.

They cannot directly replace the seaworthiness screening of each cargo lot in cross-port voyages of semi-submersible ships.

In summary, existing studies have advanced tramp ship voyage scheduling and advanced speed and fuel consumption optimization. They have further advanced stowage stability and ballast operation modeling. However, few studies focus on semi-submersible ship transportation. This transportation carries one lot of heavy-lift cargo per leg. Therefore, the main contributions of this paper are as follows. (1) To address the joint optimization of heavy-lift cargo stowage and speed decisions during transportation by semi-submersible ships, this paper comprehensively considers factors such as cargo mass, loading and unloading time windows, ship deadweight, and speed range. The objective function is set to minimize the total transportation cost. A joint optimization model of voyage and speed is constructed for semi-submersible ships. This model considers the loading safety of heavy-lift cargo. (2) A two-stage algorithm is designed. In the second stage, ship GM is linearized. An exact algorithm and a heuristic algorithm are combined. They solve the joint optimization model of voyage and speed for semi-submersible ships. This model considers the loading safety of heavy-lift cargo.

The remainder of this paper is structured as follows: Section 2 constructs a joint optimization model of voyage and speed for semi-submersible ships. This model considers the loading safety of heavy-lift cargo. Section 3 presents the method design of the two-stage algorithm. Section 4 presents the comparison of solution methods and a case study. It also provides some managerial insights for entrepreneurs. Finally, Section 5 is the conclusion.

2. Mathematical Model

2.1. Problem Statement

During navigation, semi-submersible ships adjust the ballast water amount according to cargo mass. They control the ship floating condition and maintain stability. When the cargo mass is excessive, even after all ballast water is discharged, the ship may still fail to meet the navigable draft requirements, because its draft exceeds the navigational limit or its reserve buoyancy is insufficient. At the same time, discharging all ballast water weakens ship stability. This may cause cargo shifting or ship capsizing. Therefore, the cargo mass and its stowage pattern affect the floating condition, stability, and transportation safety of semi-submersible ships. This paper studies the joint optimization of heavy-lift cargo stowage and speed decisions during transportation by semi-submersible ships. It constructs a joint optimization model of voyage and speed for semi-submersible ships. The objective function is set to minimize the total transportation cost. This model considers the loading safety of heavy-lift cargo.

In the problem modeling, the set of loading ports of all cargo is denoted as $\mathcal{P}$. The set of unloading ports is denoted as $\mathcal{D}$. Ship k transports cargo r from loading port h to unloading port e according to its loading and unloading requirements. Directed transportation arcs between nodes represent routes. Each arc is associated with the loading and unloading time window of the cargo. Ship stability is quantified by the GM after free-surface correction, which is used as a key safety indicator. The GM value of the ship under various loading and ballast conditions meets the minimum stability requirement.

In terms of the loading safety of heavy-lift cargo, the setting of the GM value affects the cargo stowage scheme. When the set minimum GM limit is large, it may reduce the quantity of transported cargo. The operating profit of the enterprise is then low. When the set minimum GM limit is small, the quantity of cargo stowed on the ship increases. But navigation safety is low. Safety accidents easily occur. At the same time, cargo stowage directly affects ship stability and the loading condition. It affects the feasible range of speed decisions through factors such as draft and navigation resistance. Speed affects the voyage

time and fuel consumption. It further affects the total transportation cost and the satisfaction of time window constraints. Therefore, on the premise of ensuring ship transportation safety, this paper jointly optimizes cargo stowage and the ship speed to achieve overall optimality of the transportation scheme in terms of both economy and safety.

Before establishing the mathematical model, the following assumptions are made:

(1) Loading and unloading of semi-submersible ships usually take place in relatively calm port waters. They do not approach the inner sea area of the port. Therefore, they do not occupy berth resources. They do not face the situation of waiting for berths. They do not need to consider the impact of wind and waves. They can complete loading and unloading operations within 24 h.

(2) This study is limited to the operational planning level. The cargo mass, height of center of gravity, and initial metacentric height are used as criteria to measure whether the loading requirements can be satisfied, without considering the complete verification process, including stability at large angles of heel, which still needs to be completed before actual transportation.

(3) Each transportation task can only carry one lot of cargo. It is not allowed to load other cargo during transportation.

2.2. Parameters and Variables

The parameters and variables used to form the mathematical model are given in Table 1.

Table 1. Parameters and variables.

Types	Notations	Descriptions
Sets	$\mathcal{R}$	Set of all cargo r.
	$\mathcal{K}$	Set of all ships k.
	M_k	Set of all ballast tanks m of ship k.
	$\mathcal{P}$	Set of loading port nodes, $\mathcal{P} = \{1, 2, \dots, n\}$.
	$\mathcal{D}$	Set of unloading port nodes, $\mathcal{D} = \{n+1, n+2, \dots, 2n\}$, where $n+h$ is the unloading port node corresponding to loading port node h.
Decision variables	x_{ehk}	0–1 variable: if ship k sails from h to e, $x_{ehk} = 1$; otherwise, $x_{ehk} = 0$.
	(x_{rk}, y_{rk}, z_{rk})	Center-of-gravity coordinates of cargo r loaded on ship k.
	θ_{km}	Ballast coefficient of the m-th ballast tank of ship k.
Auxiliary variables	Q_{hk}^{Z}	Cargo mass loaded on ship k when it arrives at loading port h.
	Q_{ek}^{X}	Cargo mass loaded on ship k when it arrives at unloading port e.
Parameters	h, e	Loading port and unloading port corresponding to cargo r, respectively. $h, e \in \mathcal{P} \cup \mathcal{D}$.
	Z	Total transportation cost.
	W_k, (x_k, y_k, z_k)	Lightship weight of ship k and its center-of-gravity coordinates.
	Δ_k	Displacement of ship k in laden condition.
	n	Number of lots of all cargo r.
	GM_{rk}	GM of semi-submersible ship after free-surface correction for cargo r on ship k.
	KB_k	Height of center of buoyancy of ship k.
	x_{kf}	x-coordinate of ship k in upright floating condition.
	BM_k	Transverse metacentric radius of ship k.
	GM_L	Minimum limit of GM of semi-submersible ship after free-surface correction.
	KG_{rk}	Center-of-gravity height of the overall ballast water after ship k loads cargo r.

Table 1. *Cont.*

Types	Notations	Descriptions
Parameters	FR_k	Correction value of free surface in ballast tanks of ship k to initial stability.
	B_{km}	Maximum ballast water amount of the m-th ballast tank of ship k.
	$(x^{\mathrm{B}}_{km}, y^{\mathrm{B}}_{km}, z^{\mathrm{B}}_{km})$	Center-of-gravity coordinates of the m-th ballast tank of ship k under full tank condition.
	z^{L}_{km}	z-coordinate of the tank bottom of the m-th ballast tank of ship k.
	I_{km}	Transverse moment of inertia of the free surface area of ship k about its inclination axis.
	ρ	Seawater density.
	α_{km}	Auxiliary variable.
	J_k	Radius of gyration in roll of ship k.
	T_{rk}	Rolling period of ship k after loading cargo r.
	T^{U}_k, T^{L}_k	Upper and lower limits of rolling period of ship k.
	GM_{L}	Minimum initial stability limit of ship in laden condition.
	$s(k)$, $d(k)$	Virtual origin and virtual destination of ship k, respectively.
	Q_r	Cargo mass of cargo r.
	C_k	Maximum cargo mass that ship k can carry.
	t_{ehvk}	Total time for ship k to sail from port h to e at speed v.
	$[t_{ah}, t_{bh}]$	Time window for cargo arrival at loading port h.
	v_{ehk}	Speed of ship k sailing from node h to node e.
	L_{ehk}	Sailing distance of ship k from node h to node e.
	v_{kL}, v_{kU}	Minimum and maximum speeds of ship k.
	F_{ehk}	Fuel consumption of ship k on route (h, e).
	C	Unit fuel cost.
	α^Z_k	Port cost of ship k at loading port h.
	α^X_k	Port cost of ship k at unloading port e.
	G_k	Unit charter cost of ship k.
	D_k	Number of days used by ship k.
	φ	Influence coefficient of ship deadweight on main engine fuel consumption.
	D^F_k	Rated deadweight of ship k.
	P_k	Main engine power of ship k under common operating conditions.
	g_k	Fuel consumption rate of the main engine of ship k under common operating conditions.

2.3. Modeling

To facilitate the description of the position information of each ballast tank and cargo of a semi-submersible ship, a ship coordinate system is established. The intersection of the after perpendicular and the base plane is taken as the coordinate origin o. The intersection line of the base plane and the centerline plane is the x-axis. Its positive direction points to the bow. The after perpendicular is the z-axis. Its positive direction points upward. The line passing through the coordinate origin and perpendicular to the xoz plane is the y-axis. Its positive direction points to starboard. Based on this, a joint optimization model of voyage and speed for semi-submersible ships considering the loading safety of heavy-lift cargo is established as follows:

$$\min Z = \sum_{k\in\mathcal{K}} \sum_{(h,e)\in\mathcal{P}\cup\mathcal{D}} CF_{ehk}x_{ehk} + \sum_{h\in\mathcal{P},e\in\mathcal{D}} (\alpha^Z_k + \alpha^X_k)x_{ehk} + \sum_{k\in\mathcal{K}} G_k D_k \quad (1)$$

$$\text{s.t. } F_{ehk} = \left[\varphi + \frac{(1-\varphi)Q^Z_{hk}}{D^F_k}\right]\frac{L_{ehk}}{v_{ehk}}P_k g_k \quad (2)$$

$$\sum_{k\in\mathcal{K}}\sum_{e\in\mathcal{D}} x_{ehk} = 1,\ h \in \mathcal{P} \tag{3}$$

$$\sum_{e\in\mathcal{R}} x_{s(k)ek} = 1 \tag{4}$$

$$\sum_{e\in\mathcal{R}} x_{ehk} - \sum_{e\in\mathcal{R}} x_{ehk} = 0,\ h \in \mathcal{P}\cup\mathcal{D}\backslash\{s(k), d(k)\} \tag{5}$$

$$\sum_{h\in\mathcal{R}} x_{hd(k)k} = 1 \tag{6}$$

$$Q_r \le C_k,\ r \in \mathcal{R}, k \in \mathcal{K} \tag{7}$$

$$Q_{hk}^{Z} = 0,\ h \in \mathcal{P}, k \in \mathcal{K} \tag{8}$$

$$Q_{ek}^{X} = 0,\ e \in \mathcal{D}, k \in \mathcal{K} \tag{9}$$

$$x_{ehk}(t_{hk} + t_{ehk} - t_{ek}) \le 0,\ h, e \in \mathcal{P}\cup\mathcal{D}, k \in \mathcal{K} \tag{10}$$

$$t_{ah} \le t_{hk} \le t_{bh},\ h, e \in \mathcal{P}\cup\mathcal{D}, k \in \mathcal{K} \tag{11}$$

$$v_{kL} \le v_{ehk} \le v_{kU},\ h, e \in \mathcal{P}\cup\mathcal{D}, k \in \mathcal{K} \tag{12}$$

$$GM_{rk} \ge GM_L,\ r \in \mathcal{R}, k \in \mathcal{K} \tag{13}$$

$$GM_{rk} = KB_k + BM_k - KG_{rk} - FR_k \tag{14}$$

$$KG_{rk} = [\sum_{m\in\mathcal{M},k\in\mathcal{K}} B_{km}\theta_{km}(z_{km}^{\mathrm{B}}\theta_{km} - z_{km}^{\mathrm{L}}\theta_{km} + z_{km}^{\mathrm{L}}) + w_r z_{rk} + w_k z_k]/\Delta_k \tag{15}$$

$$FR_k = \sum_{m\in\mathcal{M},k\in\mathcal{K}} \gamma_m(1-\gamma_m) I_m \rho/\Delta_k \tag{16}$$

$$\sum_{m\in\mathcal{M},k\in\mathcal{K}} B_{km}\theta_{km} + Q_r + w_k \le \Delta_k,\ r \in \mathcal{R} \tag{17}$$

$$\sum_{m\in\mathcal{M},k\in\mathcal{K}} B_{km}\theta_{km}x_{km}^{\mathrm{B}} + Q_r x_{rk} + w_k x_k = \Delta x_{kf},\ r \in \mathcal{R} \tag{18}$$

$$\sum_{m\in\mathcal{M},k\in\mathcal{K}} B_{km}\theta_{km}y_{km}^{\mathrm{B}} + Q_r y_{rk} + w_k y_k = 0,\ r \in \mathcal{R} \tag{19}$$

$$T_{rk} = 2J_k/\sqrt{GM_{rk}} \tag{20}$$

$$T_k{}^{\mathrm{L}} \le T_{rk} \le T_k{}^{\mathrm{U}},\ k \in \mathcal{K} \tag{21}$$

$$0 \le \theta_{km} \le 1,\ \forall m \in \mathcal{M}, k \in \mathcal{K} \tag{22}$$

$$x_{ehk} \in \{0, 1\},\ h, e \in \mathcal{P}\cup\mathcal{D}, k \in \mathcal{K} \tag{23}$$

where Equation (1) is the objective function. It minimizes the total transportation cost during transportation. The shipping cost includes a fixed cost and voyage cost. For the shipping cost, the fixed cost is assumed to be constant within a time period. Therefore, the objective function consists of three terms. The first term is the fuel cost of the semi-submersible ship during navigation. The second term is the port cost. The third term is the charter cost. Equation (2) is the calculation formula for fuel consumption. Equation (3) ensures that all heavy-lift cargo can be transported. Equation (4) means that the cargo-carrying semi-submersible ship needs to depart from the virtual origin once. Equation (5) is the integrity constraint of the transportation route of ship k. Equation (6) means that the cargo-carrying ship k needs to arrive at the virtual destination once. Equation (7) means that the cargo mass Q_r to be transported cannot exceed the maximum cargo mass C_k that

ship k can carry. Equation (8) means that ship k has no cargo loaded when it arrives at loading port h. Equation (9) means that ship k has no cargo loaded when it leaves unloading port e. Equation (10) means that the arrival time of the ship at e is later than its departure time from h. The difference is the time for the ship to sail from h to e. Equation (11) is the time window constraint. It ensures that the ship arrives at the corresponding node within the specified time. Equation (12) is the speed constraint. It ensures that the ship sails within the specified speed range. Equation (13) means that the GM, as a ship safety indicator, must be greater than the minimum GM limit. Equation (14) gives the calculation formula for the GM of the semi-submersible ship after free-surface correction, denoted as GM_{rk}. This is the ship safety indicator formula. Each lot of cargo h loaded on each ship k corresponds to a GM_{rk}. Equation (15) is the calculation formula for the center-of-gravity height of the ship, cargo, and ballast water as a whole. Equation (16) is the correction value of the free surface in the ballast tank to initial stability. $\lceil \cdot \rceil$ is the ceiling function. When the ballast tank is empty or full, $\lceil \gamma_m(1-\gamma_m) \rceil$ is 0. In other states, it is 1. Equation (17) is the ship displacement limit. That is, the sum of ballast water weight, cargo weight, and lightship weight cannot exceed the ship displacement. Equations (18) and (19) are equilibrium constraints that ensure the ship is upright in the x and y directions, respectively. Equation (20) describes the relationship between the ship rolling period and initial stability. Equation (21) is the ship rolling period constraint. Equation (22) is the decision variable constraint. Equation (23) is the 0–1 variable constraint.

3. Solution Method

For the joint optimization problem of voyage and speed for semi-submersible ships considering the loading safety of heavy-lift cargo, this paper designs a two-stage solution algorithm. It solves the original model in stages. This improves the solution efficiency of the model.

In the first stage, the main task is to complete the initial allocation of heavy-lift cargo and the construction of a feasible solution. Basic constraints of cargo and ships are used to construct an initial feasible solution. The objective function is to minimize total transportation cost. Then, a global search algorithm is used to iteratively optimize the initial solution. One-way insertion and two-way exchange strategies are adopted. They dynamically adjust the cargo allocation scheme. They also optimize the navigation cost of each leg.

In the second stage, the main tasks are safety assessment, cargo reallocation, and speed optimization. Based on the cargo allocation results output by the first stage, the allocated cargo is checked for safety. This check combines the operation safety constraints of semi-submersible ships. Some cargo fails the safety check. This cargo is preferentially reassigned to semi-submersible ships with higher deadweight. If it still fails to satisfy the constraints, it is removed. In the second stage, the safety check and adjustment results are fed back to the first stage. The first stage continues to perform cargo allocation and speed optimization. The two stages alternate iteratively. This continues until the current scheme satisfies GM safety constraints. The total cost also converges. Then, the optimal cargo allocation and speed scheme is output. The specific solution process is shown in Figure 1.

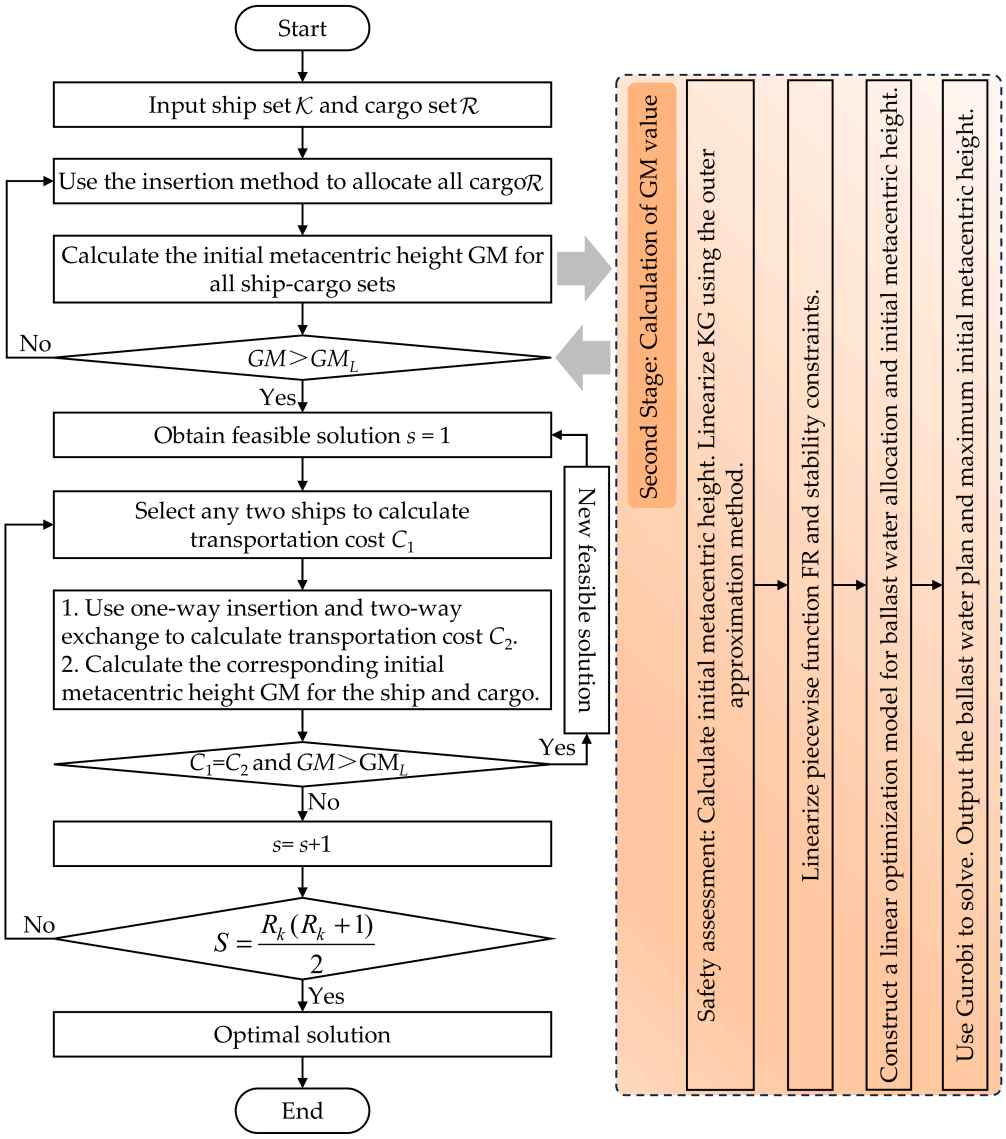


Figure 1. Framework of the two-stage algorithm.

3.1. First Stage

Initial cargo allocation determines the heavy-lift cargo carried by each ship. This allocation process needs to comprehensively consider multiple constraints. These constraints include the specified loading and unloading time windows of each cargo, the speed range of the ship, and the operation rule of "carrying only one lot of cargo per voyage". Under the condition of satisfying all the above constraints, the goal is to match semi-submersible ships for heavy-lift cargo transportation. To solve this complex combinatorial allocation problem, this study uses the insertion method to construct an initial allocation scheme. All cargo to be allocated is sorted in ascending order according to the latest allowed loading time t_{bh} of each cargo r. Cargo is numbered $r = 1, 2, 3, \ldots, n$ in this order. The allocation process follows the steps below:

Step 1 According to the cargo code, the corresponding loading port code of the cargo is $\mathcal{P} = \{1, 2, 3, \ldots, n\}$. The corresponding unloading port code is $\mathcal{D} = \{n + 1, n + 2, \ldots, 2n\}$. Therefore, cargo r can be represented by the four-element basic information in the Figure 2.

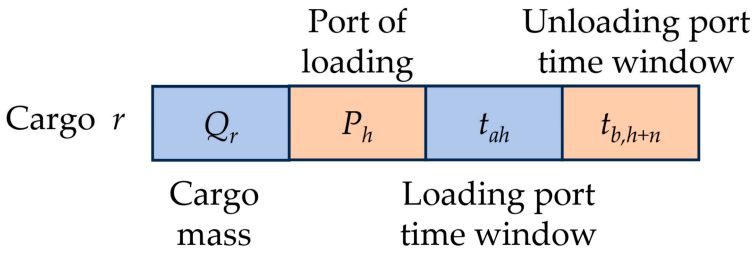


Figure 2. Basic information of cargo r.

Step 2 Use the insertion method to allocate cargo 1 to n to k semi-submersible ships. Construct an initial feasible solution. Assume that cargo r has been allocated to semi-submersible ship k. Then, cargo s $(s > r)$ is to be allocated to semi-submersible ship k and transported after cargo r. It needs to satisfy the following conditions:

$$Q_s \le C_k \tag{24}$$

$$v_{KL} \le \frac{L_{r+n}}{t_{be} - t_{a,r+n}} \le v_{KU},\ r,\ s \in \mathcal{D} \tag{25}$$

Step 3 Judge the safety of the ship during cargo transportation. The specific process is as follows:

(a) For cargo r, the initial metacentric height GM_{rk} of the ship when it transports this cargo should be calculated.
(b) If $GM_{rk} \ge GM_L$, go to (d). Otherwise, go to (c).
(c) The algorithm stows cargo r on a semi-submersible ship with larger tonnage. If $GM_{rk} \ge GM_L$, go to (d). Otherwise, remove the cargo.
(d) This allocation scheme is feasible in terms of safety. Output the allocation scheme.
(e) Let this allocation scheme be $s = 1$.

Step 4 Perform a global search solution on this allocation scheme. Optimize the allocation scheme using one-way insertion and two-way exchange. The specific process is as follows:

(1) One-way insertion

One-way insertion means inserting one lot or several adjacent lots of cargo from Ship A into the cargo transportation plan of Ship B. As shown in Figure 3, the 2nd and 3rd lots of cargo of Ship A are inserted between the 2nd and 3rd lots of cargo of Ship B for transportation.

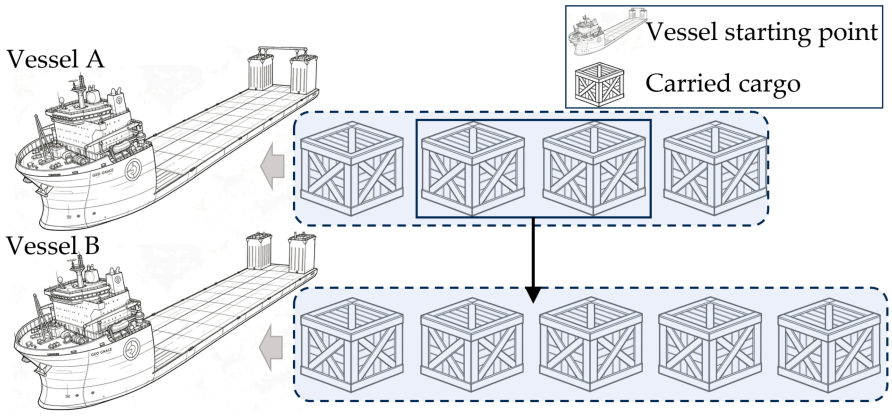


Figure 3. Schematic diagram of one-way insertion.

(2) Two-way exchange

Two-way exchange means that one lot or several adjacent lots of cargo transported by Ship A and Ship B are exchanged for transportation. As shown in Figure 4, it indicates that the 2nd and 3rd lots of cargo of Ship A are exchanged with the 2nd, 3rd, and 4th lots of cargo of Ship B for transportation.

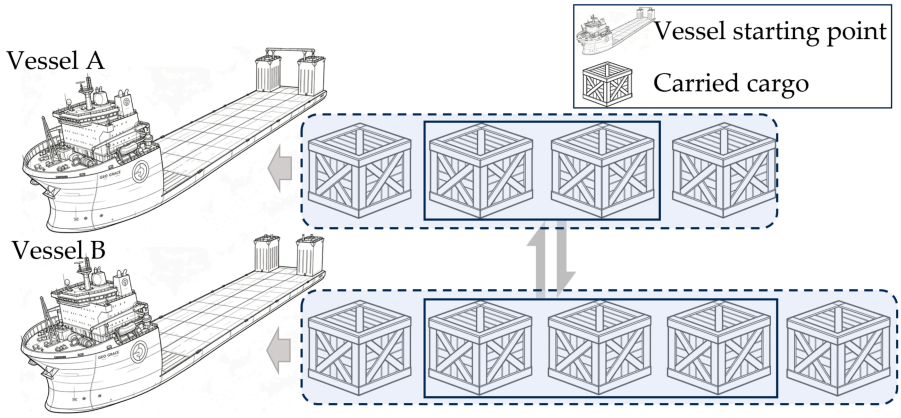


Figure 4. Schematic diagram of two-way exchange.

Cargo of one ship can be inserted into another ship for transportation. Or part of the cargo on two ships can be exchanged to the other ship for transportation. This needs to satisfy four conditions:

(a) The mass of heavy-lift cargo cannot exceed the deck cargo capacity of the semi-submersible ship to be inserted;
(b) The time window constraint can be satisfied after insertion;
(c) The GM limit can be satisfied after insertion;
(d) The speed change in some transportation arcs caused by inserting a new task can satisfy the speed limit requirement.

If the conditions are not satisfied, judge which condition the cargo fails. If it fails conditions (a) and (b), the cargo should be allocated to a ship with larger deadweight. If this ship still fails, a new ship should be inserted. If the current ship fails condition (c), the cargo should be allocated to a ship with larger deadweight. If this ship is still not suitable, the cargo should be removed. If the current ship fails condition (d), the speed limit should be appropriately increased.

Step 5 The speed of each leg should be optimized as a decision variable. Fuel consumption should be calculated. Then the total ship operating cost should be obtained.

Step 6 The cost before and after insertion or exchange is compared. If the cost increases, go to Step 4. If the cost is reduced, replace the original allocation scheme with the new cargo allocation scheme after insertion and exchange. Let $s = s + 1$. Then, go to Step 4. The calculation should be stopped and the result should be output when the total cost does not change.

3.2. Second Stage

After generating the initial feasible solution, it is necessary to solve the ship safety constraint problem for the initial feasible solution according to the constraint method. The GM value is calculated. Safety assessment is performed on the ship. The ship safety indicator is determined by the initial metacentric height GM_{rk} of the semi-submersible ship after free-surface correction. In Formula (14), KG_{rk} and FR_{rk} are nonlinear terms. They need to be linearized before solving. The specific steps are as follows:

Step 1 Linearize KG_{rk} using the outer approximation method. Extract the nonlinear part U_{km} from it. The formula is as follows:

$$U_{km} = B_{km}(z_{km}^{\mathrm{B}} - z_{km}^{\mathrm{L}})(\theta_{km})^2 + B_{km}z_{km}^{\mathrm{L}}\theta_{km},\ \forall m \in \mathcal{M},\ k \in \mathcal{K} \tag{26}$$

The process of converting U_{km} into a linear piecewise function is as follows. The meanings of the parameters involved in the process are as follows: u_{km} is the derivative function of U_{km}. $\theta_{km}^{\max}$ and $\theta_{km}^{\min}$ are the maximum and minimum values of θ_{km}, respectively. $U_{km}^{\max}$ and $U_{km}^{\min}$ are the function values of U_{km} at $\theta_{km}^{\max}$ and $\theta_{km}^{\min}$, respectively. $u_{km}^{\min}$ is the function value of u_{km} at $\theta_{km}^{\min}$. Ψ_k is the set of line segment parameters after U_{km} is converted into a linear piecewise function. L_{ka}^k, L_{kb}^k and L_{kt}^k represent the slope, intercept, and abscissa of the tangent point of the line segment, respectively. ζ_{km} is the number of line segments in Ψ_k obtained after the linear transformation of U_{km}. U_{km}^n is U_{km} at the n-th iteration of the algorithm. θ_{km}^n is θ_{km} at the n-th iteration of the algorithm. ε_{KG} is the absolute error of KG_{rk}. ε_u is the absolute error of U_{km}.

(a) Input U_{km} and u_{km}, $\theta_{km}^{\max}$ and $\theta_{km}^{\min}$. Let $\Psi_k = \emptyset$, $n = 1$, $U_{km}^n = U_{km}^{\max} - \varepsilon_u$, $\theta_{km}^m = \theta_{km}^{\max}$.

(b) If $(U_{km}^{\min} - U_{km}^k)/(\theta_{km}^{\min} - \theta_{km}^k) \le u_{km}^{\min}$, let $L_{ka}^n = u_{km}^{\min}$, $L_{kb}^n = U_{km}^{\min} - u_{km}^{\min} \cdot \theta_{km}^{\min}$, $L_{kt}^n = \theta_{km}^{\min}$, $\Psi_k = \Psi_k \cup [L_{ka}^k, L_{kb}^k, L_{kt}^k]$, go to (f). Otherwise, go to (c).

(c) Calculate the tangent point between U_{km} and the straight line passing through the point $(\theta_{km}^n, U_{km}^n)$. Obtain the abscissa L_{kt}^n of the tangent point. See Equation (27). Then, $L_{ka}^n = u_m(L_{kt}^n)$, $L_{kb}^n = U_{km}(L_{kt}^n) - u_m(L_{kt}^n) \cdot L_{kt}^n$, $\Psi_k = \Psi_k \cup [L_{ka}^n, L_{kb}^n, L_{kt}^n]$. Go to (d).

$$L_{kt}^n = \theta_{km}^n - \sqrt{(\theta_{km}^n)^2 - \frac{U_{km}^n - B_{km}z_{km}^{\mathrm{L}}\theta_{km}^n}{B_{km}(z_{km}^{\mathrm{B}} - z_{km}^{\mathrm{L}})}} \tag{27}$$

(d) If $L_{ka}^n\theta_{km}^{\min} + L_{kb}^n < U_{km}^{\min} - \varepsilon_u$, let $n = n + 1$, and go to (e). Otherwise, go to (f).

(e) Solve $L_{ka}^{n-1}L_{kt}^n + L_{kb}^{n-1} = U_{km}(L_{kt}^n) - \varepsilon_u$ to obtain L_{kt}^n. See Equation (28). Let $\theta_{km}^n = L_{kt}^n$, $U_{km}^n = U_{km}(L_{kt}^n) - \varepsilon_u$. Go to (c).

$$L_{kt}^n = \theta_{km}^n - \sqrt{(\theta_{km}^n)^2 - \frac{U_{km}^n - B_{km}z_{km}^{\mathrm{L}}\theta_{km}^n}{B_{km}(z_{km}^{\mathrm{B}} - z_{km}^{\mathrm{L}})}} - \sqrt{\frac{\varepsilon_u}{B_{km}(z_{km}^{\mathrm{B}} - z_{km}^{\mathrm{L}})}} \tag{28}$$

(f) Output Ψ_k. End.

From the above process, the linear piecewise function expression of U_{km} can be obtained. Equation (26) is accurately described by Equation (29). Thus, the linearization of KG is achieved.

$$U_{km} = \max\{L_{ka}^n\theta_{km} + L_{kb}^n, \forall n = 1, 2, \ldots, K_{km}\}, \forall m \in \mathcal{M}, k \in \mathcal{K} \tag{29}$$

The absolute error of KG_{rk} is ε_{KG}. Then, the allowable deviation of U_{km} is taken as $\varepsilon_u = \varepsilon_{KG}\Delta/M$. When the deviations of U_{km} are all less than ε_u, the deviation of KG_{rk} can be guaranteed not to exceed ε_{KG}.

Step 2 Use piecewise function linearization for FR.

FR contains a discontinuous piecewise function, namely Equation (16). A continuous piecewise function β_m and inequality constraint formulations are introduced, as shown below:

$$\beta_m = \begin{cases} \theta_m & 0 \le \theta_m < 0.5 \\ 1 - \theta_m & 0.5 \le \theta_m \le 1 \end{cases} \tag{30}$$

$$\alpha_m = \begin{cases} 0 & \theta_m = 0, 1 \\ 1 & 0 \le \theta_m \le 1 \end{cases} \tag{31}$$

$$\alpha_m \ge \beta_m, \forall m \in \mathcal{M} \tag{32}$$

When $0 < \theta_m < 1$, $\beta_m > 0$. At this time, Equation (32) restricts α_m to only take 1.

When $\theta_m = 0$ or 1, $\beta_m = 0$. Under the constraint of Equation (32), α_m can take 0 or 1. The objective function seeks a maximum. This imposes a requirement on Equation (31). Then, α_m tends to take 0.

For β_m, three continuous variables $\lambda_{m,r}$ ($r = 1, 2, 3$) and two 0–1 variables $\omega_{m,s}$ ($s = 1, 2$) are introduced. They are converted into linear constraints, namely Equations (33)–(41).

$$\beta_m = 0 \times \lambda_{m,1} + 0.5 \times \lambda_{m,2} + 0 \times \lambda_{m,3}, \forall m \in \mathcal{M} \tag{33}$$

$$\theta_m = 0 \times \lambda_{m,1} + 0.5 \times \lambda_{m,2} + 1 \times \lambda_{m,3}, \forall m \in \mathcal{M} \tag{34}$$

$$\sum_{r=1}^{3} \lambda_{m,r} = 1, \forall m \in \mathcal{M} \tag{35}$$

$$\sum_{s=1}^{2} \omega_{m,s} = 1, \forall m \in \mathcal{M} \tag{36}$$

$$\lambda_{m,1} \le \omega_{m,1}, \forall m \in \mathcal{M} \tag{37}$$

$$\lambda_{m,2} \le \omega_{m,1} + \omega_{m,2}, \forall m \in \mathcal{M} \tag{38}$$

$$\lambda_{m,3} \le \omega_{m,2}, \forall m \in \mathcal{M} \tag{39}$$

$$0 \le \lambda_{m,r} \le 1, \forall m \in \mathcal{M}, r = 1, 2, 3 \tag{40}$$

$$\omega_{m,s} \in \{0, 1\}, \forall m \in \mathcal{M}, s = 1, 2 \tag{41}$$

Among them, Equations (33) and (34) are the relationships between β_m, θ_m and the newly introduced variables. Equation (35) restricts the sum of $\lambda_{m,r}$ to be 1. Equation (36) requires that only one $\omega_{m,s}$ can be 1. Equations (37)–(39) are the relationships between $\lambda_{m,r}$ and $\omega_{m,s}$. Equation (40) is the range constraint of the continuous variable $\lambda_{m,r}$. Equation (41) constrains the value range of the variables.

Step 3 Linearize the GM_{rk} constraint.

When $GM_{ik} \le 0$, Equation (20) leads to no feasible solution. When $0 \le GM_{ik} < GM_L$, Equation (13) leads to no feasible solution. At this time, the initial stability of the ship is insufficient. Once subjected to external disturbance, it can easily capsize. When $GM_{ik} \ge GM_L$, constraints (20) and (21) are reformulated to obtain the linear constraint of Equation (42).

$$(2J_k/{T_k}^{\mathrm{U}})^2 \le GM_{rk} \le (2J_k/{T_k}^{\mathrm{L}})^2 \tag{42}$$

Step 4 Transform the ballast water allocation and initial stability optimization model of the semi-submersible ship into a linear optimization model. This includes

$$\max GM_{rk} = KB_k + BM_k - KG_{rk} - FR_k \tag{43}$$

$$\text{s.t. } KG_{rk} = [\sum_{m \in M, k \in K} U_{km} + Q_r z_{rk} + w_k z_k]/\Delta \tag{44}$$

Equations (13)–(19), (22), (29), (32)–(42)

Step 5 The linear optimization model in Step 4 is solved by linear solvers such as Gurobi. This solver can quickly obtain the optimal ballast water allocation scheme and the corresponding maximum initial metacentric height.

4. Case Study

4.1. Semi-Submersible Ship and Cargo Parameters

Assume that the fleet consists of seven semi-submersible ships. Among them, three ships have a deadweight of 28,000 tons. The other four ships have a deadweight of 50,000 tons. The ballast tank data, lightship weight and its center-of-gravity coordinates, height of center of buoyancy, and transverse metacentric radius of these two ship types are obtained from their loading manuals. The speed range of both ship types is set to 9–16 knots. We refer to the loading and unloading ports involved in the actual heavy-lift cargo transportation business of China Ocean Shipping Group and Dockwise. These ports are shown in Table 2. An initial port is assumed for each ship. These initial ports are shown in Table 3. According to historical transportation demand, the fleet needs to complete 30 heavy-lift cargo transportation demands. The cargo mass is randomly generated between 10,000 tons and 38,000 tons according to a normal distribution. This describes the differentiated distribution characteristics of cargo with different masses. The earliest loading time is randomly generated between 1 and 270 days according to a uniform distribution. The time window width is set to 5 days. Thus, the loading time window of each cargo is generated. The basic information of each cargo is shown in Table 3.

Table 2. Basic information of heavy-lift cargo.

Cargo No.	Mass (10 Thousand Tons)	Loading Port	Number	Time Window (Days)	Unloading Port	Number	Time Window (Days)
1	1.5	Freeport	1	11~16	Lagos	31	28~33
2	3.8	Cadiz	2	21~26	Antwerp	32	28~33
3	3.1	Pulau Batam	3	24~29	Fao	33	40~45
4	1.2	Okpo	4	25~30	Vyborg	34	69~74
5	2.1	Singapore	5	41~46	Picton	35	56~61
6	2.4	Brest	6	43~48	Lagos	36	57~62
7	2.6	Singapore	7	50~55	Bahrain	37	63~68
8	1.7	Okpo	8	60~65	Puerto Cabello	38	91~96
9	2.7	Koje	9	62~67	Lagos	39	98~103
10	2.4	Diamante	10	72~77	Cartagena	40	88~93
11	1	Abu Dhabi	11	85~90	Mulgrave	41	111~116
12	2.3	Okpo	12	87~92	Corpus Christi	42	120~125
13	3	Yantai	13	100~105	Angra dos Reis	43	136~141
14	2.8	Qingdao	14	104~109	Barrow Island	44	118~123
15	1.5	Abu Dhabi	15	121~126	Lagos	45	144~149
16	1.1	Singapore	16	127~132	Sharjah	46	139~144
17	2.9	Yantai	17	130~135	Hay Point	47	144~149
18	0.9	Rotterdam	18	141~146	Hammerfest	48	146~151
19	1.6	Jebel Ali	19	141~146	Dundee	49	166~171
20	1.9	Laem chabang	20	144~149	Batangas	50	149~154
21	2.1	Pori	21	163~168	Corpus Christi	51	185~190
22	2.4	Okpo	22	167~172	Corpus Christi	52	186~191
23	1.6	Singapore	23	168~173	Veracruz	53	212~217
24	2.7	Houston	24	176~181	Sharjah	54	211~216
25	1.5	Houston	25	188~193	Rotterdam	55	203~208
26	2.8	Pulau Batam	26	201~206	Qingdao	56	209~214
27	1.2	Qingdao	27	217~222	Nepoui	57	232~237
28	3.7	Taicang	28	230~235	Manzanillo	58	254~259
29	1.4	Ulsan	29	234~239	Pulau Batam	59	246~251
30	1.3	Pasir Panjang	30	253~258	Perth	60	263~268

Table 3. Basic information of ships.

Ship k	1	2	3	4	5	6	7
Deadweight (10^4 DWT)	2.8	2.8	2.8	5	5	5	5
Initial position	Lagos	Sharjah	Bahrain	Lagos	Sharjah	Bahrain	Cartagena

4.2. Optimization Results and Analysis

To verify the effectiveness of the two-stage algorithm designed in this paper, a comparison scheme based on manual experience is set up. It is denoted as Scheme I. Scheme I strictly satisfies all constraints of the model. These constraints include ship deadweight, loading and unloading time windows, speed range, and GM safety limit. It takes the distance between semi-submersible ships and loading/unloading ports as the main decision basis. It also takes loading and unloading time requirements as the main decision basis. The cargo allocation and speed scheme is formulated by manual experience. The cargo allocation and speed optimization results obtained by the two-stage algorithm in this paper are denoted as Scheme II. In this paper, the convergence tolerance for the change in the objective function value is set to 1×10^{-6}. It is used as the termination condition of the algorithm. The algorithm becomes stable after 835 iterations. After a runtime of 111.7 s, it obtains the optimized solution under the current algorithm search conditions. During the run, the cumulative number of accepted moves by all operators is 103. The cost curve of the iterative one-way insertion and two-way exchange designed in this paper is shown in Figure 5. The specific results obtained by Scheme I and Scheme II are shown in Tables 4 and 5.

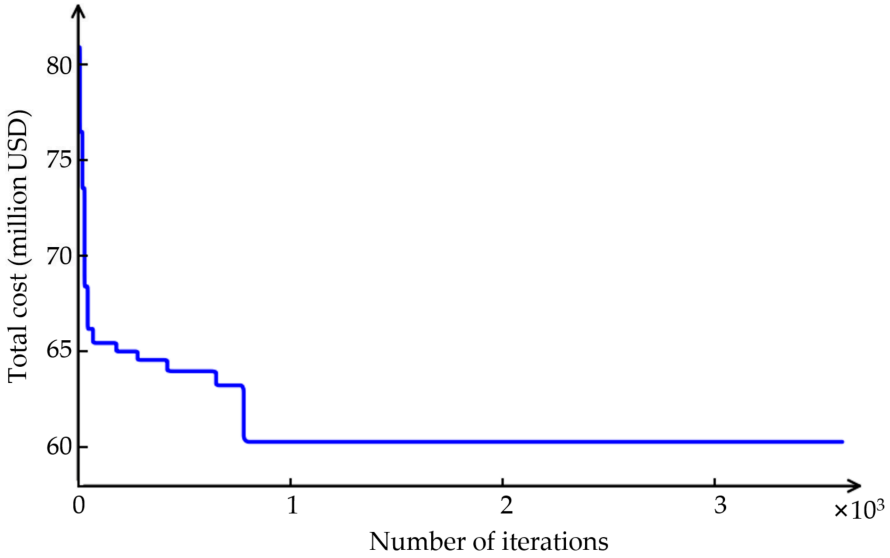


Figure 5. Cost iteration curve.

Table 4. Cost comparison between Scheme I and Scheme II.

Category	Charter Cost (Million USD)	Fuel Cost (Million USD)	Port Cost (Million USD)	Total Cost (Million USD)
Scheme I	24.42	49.78	1.75	75.95
Scheme II	23.67	35.10	1.50	60.27

As shown in Figure 5, the transportation cost exhibits a clear downward trend. It gradually becomes stable. It finally converges to the optimal cost state. In the initial iteration stage, cargo allocation and speed setting are not fully coordinated. The total cost is relatively high. As one-way insertion and two-way exchange operations continue, the model gradually finds a better cargo combination and speed configuration. The cost is reduced successively. The optimized total cost is about 20.7% lower than that of the initial scheme. The fuel cost is reduced most significantly, reaching 29.5%. The charter cost and port cost are also reduced by 3.1% and 14.3%, respectively. This result fully shows that the joint effect of speed optimization and cargo allocation has a significant effect on reducing the transportation

cost. It also verifies the effectiveness and practicality of the proposed two-stage algorithm in solving complex multi-constraint optimization problems.

Table 5. Transportation route results of each ship under Scheme I and Scheme II.

Item	Ship No.	Transportation Route	Average Speed (Knots)	GM Value (m) per Leg	Sailing Distance (Nautical Miles)	Ballast Distance (Nautical Miles)	Ballast Rate (%)
Scheme I	1	1→8→16→25	12.5	1.84→1.51→2.43→1.84	53,893	32,108	59.58
	2	4→11→18→27	11.1	2.34→2.45→2.51→2.34	50,687	25,669	50.64
	3	6→12→19→24	10.9	1.31→1.44→1.79→1.27	36,643	14,614	39.88
	4	2→15→23→29→30	12.5	1.07→2.80→2.74→2.86→2.99	33,250	16,232	48.82
	5	7→13→21→26	13.1	1.31→1.8→2.21→1.03	42,818	19,596	45.77
	6	5→10→14→20→22	13.3	2.21→1.75→1.03→1.83→1.75	38,369	17,239	44.93
	7	3→9→17→28	13.4	1.43→1.78→1.74→1.08	49,081	21,508	43.82
Scheme II	1	8→16→27→30	11.6	1.51→2.43→2.34→2.07	38,832	19,429	50.03
	2	4→11→18→23→29	10.4	2.34→2.45→2.51→1.79→1.99	50,519	14,500	28.70
	3	1→15→25	11.2	1.84→1.84→1.84	26,180	10,770	41.14
	4	7→12→19→26	12.0	1.31→1.78→2.74→1.03	39,968	17,673	44.22
	5	3→9→17→21	11.2	1.43→1.78→1.74→2.21	43,118	18,232	42.28
	6	6→13→24	12.6	1.75→1.8→1.78	44,085	19,453	44.13
	7	5→10→14→20→22	12.7	2.21→1.75→1.03→1.83→1.75	37,131	16,001	43.09

Table 4 shows that the two-stage algorithm reduces all cargo transportation costs. Among them, the voyage time is shortened. This leads to a reduction of USD 0.75 million in charter cost. This result indicates that joint optimization of route and speed can effectively reduce the ballast rate of ships. Thus, it reduces ship charter cost. The reduction in fuel cost is closely related to the strategic adjustment of speed. This reflects that reasonably setting the economic speed has a significant effect on reducing fuel consumption. It provides a basis for enterprises to formulate economic speed strategies and optimize resource allocation. Compared with Scheme I, the total cost obtained by the two-stage algorithm is reduced by USD 15.68 million. This result is achieved under the premise of strictly implementing the GM safety standard and removing cargo that does not meet stability requirements. Therefore, the above experimental results verify the effectiveness of the proposed algorithm. The specific transportation routes of the two schemes are shown in Table 5.

Table 5 shows that Scheme II obtained by the proposed algorithm is significantly better than Scheme I in terms of safety and operating economy. This scheme strictly guarantees ship stability constraints. It effectively improves ship utilization efficiency and reduces the overall operating cost. This is achieved through joint optimization of route and speed.

In terms of safety, Scheme II strictly follows the GM safety threshold. It removes cargo that does not meet requirements (No. 2 and No. 28). This ensures that all 28 allocated cargoes satisfy ship stability constraints. The GM value of each ship after free-surface correction is higher than the specified minimum limit. The GM values of some ships are further improved. This fundamentally eliminates the capsizing risk caused by insufficient stability. Transportation operation safety is strictly guaranteed.

In terms of operating efficiency, joint optimization of route and cargo allocation significantly improves ship utilization efficiency. For example, the number of cargo items transported by Ship 2 and Ship 7 increases by one for each ship. The average speed of most ships is reduced. The overall speed of the fleet is reduced by 5.88% on average. For example, the average speed of Ship 1 is reduced from 12.5 kn to 11.6 kn. This makes it more economical. This result benefits from the optimized setting of speed for laden legs in the model. It effectively shortens the voyage time. The corresponding total sailing distance of ships is significantly reduced. The ballast rate of ships is generally reduced. The ballast rate of Ship 2 is reduced from 50.64% to 28.7%. The ballast rate of Ship 4 is reduced from 48.84%

to 44.22%. This reflects that the integrated optimization of cargo allocation and the route effectively reduces the ballast voyage distance. It improves the overall operating economy.

4.3. Discussion

4.3.1. Effect of Minimum GM Limit on Cargo Allocation Scheme

GM is a key indicator for ensuring navigation safety. When transporting heavy-lift cargo, ship stability is related to navigation safety. If the GM value is too small, the ship is very easy to capsize when subjected to external forces such as wind and waves during navigation. In this case, the relationship between cargo mass and GM when the small 28,000 DWT ship and the large 50,000 DWT ship transport cargo is shown in Figure 6. The effect of adjusting the minimum GM limit on the cargo allocation scheme is shown in Figure 7.

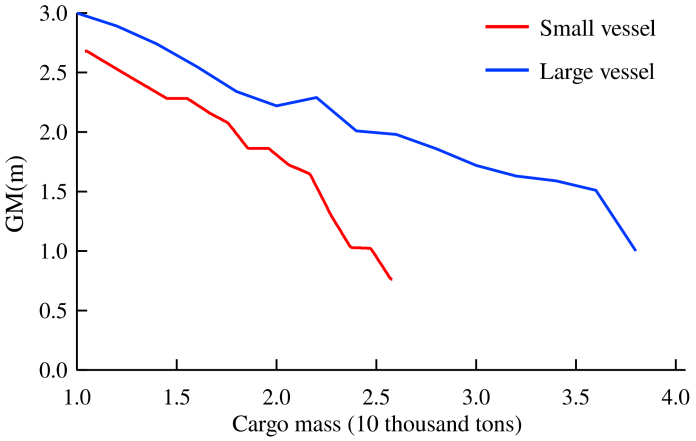


Figure 6. Relationship between cargo mass and GM.

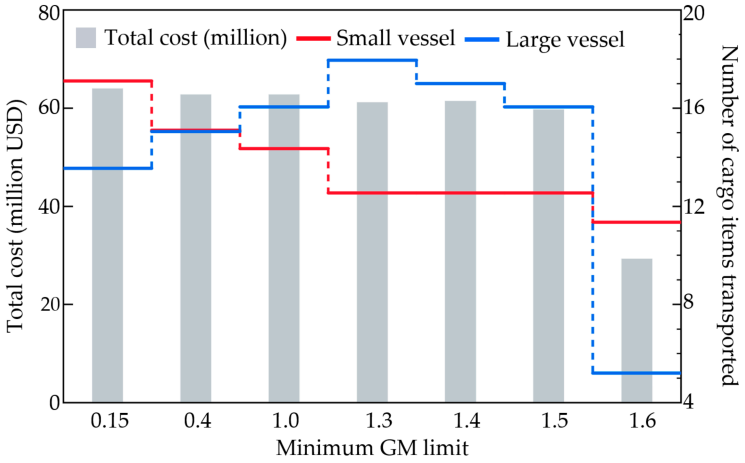


Figure 7. Effect of minimum GM limit on allocation scheme.

Figure 6 shows that the GM values of 28,000 DWT and 50,000 DWT semi-submersible ships show a monotonically decreasing trend as cargo mass increases. When the GM value is between 1.5 and 2.5 m, the ship in semi-submerged conditions can ensure a balance between safety and seaworthiness. When the cargo mass exceeds 20,000 tons, the GM value of 28,000 DWT ships rapidly approaches the safety limit. The GM value of 50,000 DWT ships still remains above the minimum limit when the cargo mass is 36,000 tons. This proves that the adaptability of 50,000 DWT ships to large-mass cargo is significantly better than that of 28,000 DWT ships. Therefore, when multiple lots of cargo are to be allocated,

large-mass cargo of 20,000 to 35,000 tons is preferentially allocated to 50,000 DWT ships. Small and medium-mass cargo below 20,000 tons is allocated to 28,000 DWT ships. This maximizes the stability advantage of 50,000 DWT ships. It also avoids 28,000 DWT ships carrying over-limit cargo. It achieves optimal ship–cargo matching. It reduces the overall transportation cost.

Figure 7 shows that adjusting different minimum GM limits has different effects on the allocation scheme in this case. When the minimum GM limit increases, the quantity of cargo carried by 28,000 DWT ships decreases. More cargo is allocated to larger ships. When the minimum GM limit is greater than 1.3 m, larger-mass cargo cannot be transported. For example, when the minimum GM limit is 1.4 m, only 29 lots of cargo out of 30 can be transported. This phenomenon indicates that the minimum GM limit plays a key screening role in cargo allocation. As the safety standard becomes stricter, the loading flexibility of ships is reduced. In particular, the transport capacity of small and medium-sized ships is significantly limited. At the same time, the increase in the GM limit also exposes a structural contradiction in ship–cargo matching. Some high-mass cargo is excluded from the transportation scheme because it cannot meet stability requirements. This reduces overall transportation efficiency.

4.3.2. Fuel Price Sensitivity Analysis

To explore the effect of shipping market fluctuations on the total cost of shipping companies, the fuel oil spot price and semi-submersible ship charter rates in the Clarkson database are both priced in USD. Based on the actual situation in the Clarkson database where the fuel oil spot price is 400–800 USD/t and semi-submersible ship charter rates change together, the cost results of shipping companies under different fuel oil spot prices are obtained, as shown in Figure 8. Based on different fuel oil spot prices, the effect of adjusting speed on the total cost before and after is analyzed, as shown in Figure 9.

Figures 8 and 9 show that fluctuations in the fuel oil spot price have a significant effect on the total transportation cost of semi-submersible ships. As the fuel price rises, the total transportation cost increases by about 18.2% on average. The proportion of fuel cost increases from 46.3% after optimization to 61.5%. It becomes a core variable affecting enterprise profitability. When the fuel price exceeds 600 USD/t, it is recommended to further reduce the economic speed by 5–8%. This is expected to additionally reduce fuel consumption by 12–15%. The total cost after speed adjustment is always lower than that before adjustment. This shows that speed optimization has continuous effectiveness in controlling total cost. When the fuel price is 400 USD/t, the cost difference is small. When the fuel price reaches 800 USD/t, the total cost after adjustment is about 15–20% lower than that before adjustment. This reflects the cost reduction advantage of speed optimization in a high-fuel-price environment. Therefore, enterprises should establish a fuel price monitoring and response mechanism. When the fuel price is high, they should actively respond to cost increase pressure by optimizing speed, reasonably adjusting the ballast strategy, and selecting economic routes. At the same time, it is recommended that shipping companies enhance the flexibility of speed management in operations. In high-fuel-price periods, they should appropriately reduce speed to greatly reduce fuel consumption. When the fuel price falls, they should moderately increase speed to guarantee the shipping schedule. This achieves a dynamic balance between cost and operating efficiency.

In summary, the collaboration between speed optimization and cargo allocation is an effective way to reduce the total cost. Research results show that by reasonably allocating cargo and optimizing speed, the fuel cost and charter cost can be significantly reduced on the premise of ensuring safety. At the same time, semi-submersible ship operating enterprises should pay attention to the limit of the GM value. They should combine ship

characteristics and cargo attributes to carry out scientific stowage and speed planning. This achieves the dual maximization of safety and economic benefits.

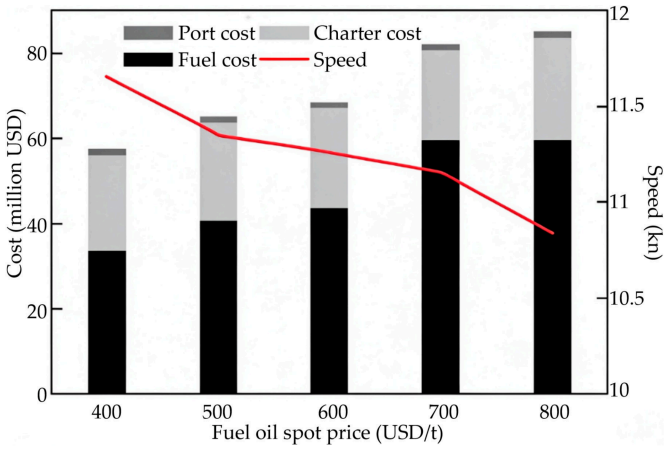


Figure 8. Effect of fuel oil spot price on various costs of shipping companies.

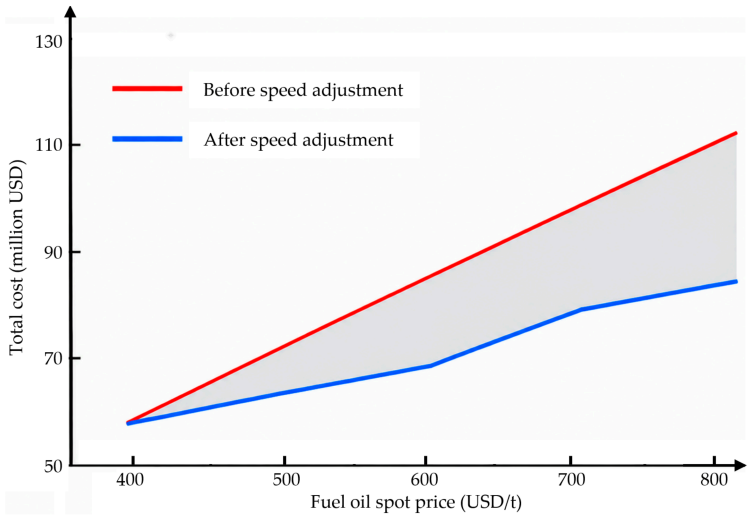


Figure 9. Effect of different fuel oil spot prices on total cost before and after speed adjustment.

5. Conclusions

Based on the existing transportation mode of semi-submersible ships for heavy-lift cargo and the shipping market, this paper studies the joint optimization problem of voyage and speed for semi-submersible ships considering the loading safety of heavy-lift cargo. The main conclusions are as follows.

(1) Real data of heavy-lift cargo in the shipping market are used to construct a correlation function among laden voyage distance, semi-submersible ship speed, and fuel consumption. The ship GM value is taken as an important constraint. On this basis, a joint optimization model of voyage and speed for semi-submersible ships considering the loading safety of heavy-lift cargo is established. A two-stage algorithm based on the model solution is designed.

(2) The actual transportation situation of a shipping company is taken as an example. The scheme obtained by the two-stage algorithm of this model is compared with the manual experience result. The manual experience result takes the distance between semi-submersible ships and loading/unloading ports and loading/unloading time

requirements as the main decision basis. The results show that the two-stage model designed in this paper can effectively reduce the cost of shipping companies by 20.7%.

(3) The sensitivity analysis results for the minimum limit of GM show that improving the minimum limit of GM reduces the compliance of small vessels for heavy-lift cargo. This may cause some heavy-lift cargo close to the maximum deadweight of small vessels to be transported by vessels with larger deadweights. This causes a tight capacity of large vessels. It may even make some cargo transportation demand difficult to satisfy. It reduces ship operating efficiency and profitability. The sensitivity analysis results for the fuel oil price show that the method designed in this paper can appropriately reduce speed when the fuel oil price runs at a high level. Rising fuel oil prices increase the enterprise fuel cost and reduce the enterprise profitability. This method mitigates these adverse effects, and it is an effective strategy for responding to the changes in fuel oil price.

Further research could be undertaken in the following directions. This paper assumes that loading and unloading operations are carried out in relatively calm port waters and can be completed within 24 h. It does not consider environmental disturbances such as port waiting and wind and waves. In reality, port waiting, wind and waves, and loading and unloading times are uncertain. Based on this paper, incorporating real-time meteorological and ocean forecasts, port congestion, and loading and unloading time uncertainty into a stochastic optimization or robust optimization framework is worth further investigation. On this basis, incorporating dynamic speed adjustment and ballast water allocation strategies of semi-submersible ships under changing sea conditions is worth further investigation to improve the safety and reliability of heavy-lift cargo transportation. In addition, this paper uses the initial metacentric height (GM) after free-surface correction as the main evaluation index for the loading safety of heavy-lift cargo on semi-submersible ships. It has not yet considered the stability at large angles of heel. Future research can further introduce evaluation indices for stability at large angles of heel. It can incorporate the constraints of both the initial stability and the stability at large angles of heel into the joint optimization model of voyage and speed for semi-submersible ships. This will further improve the safety and practical applicability of ship–cargo matching and voyage decisions.

Author Contributions: Study conception and design: R.Z. (Ruihao Zhao) and X.C.; data collection: R.Z. (Ruijia Zhao); analysis and interpretation of results: R.Z. (Ruihao Zhao) and X.C.; draft manuscript preparation: X.C. and R.Z. (Ruijia Zhao). All authors have read and agreed to the published version of the manuscript.

Funding: This research was funded by the National Natural Science Foundation of China, grant numbers 72574035 and 72204035, and the Humanities and Social Science Fund of Ministry of Education of China, grant number 24YJC630180.

Institutional Review Board Statement: Not applicable.

Informed Consent Statement: Not applicable.

Data Availability Statement: The datasets analyzed during the current study are available from the corresponding author on reasonable request.

Conflicts of Interest: The authors declare no conflicts of interest.

References

1. Petrychenko, O.; Petrichenko, I.; Yurchenko, O.; Hulak, S.; Lukosevicius, V.; Jakevicuite, G.; Skvireckas, R. Design and Development of a Unified Corporate Information System for Multimodal Transport and Logistics Companies. *Appl. Sci.* **2026**, *16*, 8366.
2. Zhang, K.; Wang, Y.; Chen, Z. A Multi-Attribute Decision-Making Approach for International Shipping Operator Selection Based on Single-Valued Neutrosophic Power Hamy Mean Operators. *Symmetry* **2024**, *16*, 706. [CrossRef]

3. Aborgela, T.; Shehata, A.S.; Kotb, M.A.; Radwan, A. Heavy Lift Semi-Submersible Ships Utilization in Offshore Wind Turbines Industry. *Energy Rep.* **2022**, *8*, 834–847. [CrossRef]
4. Rutkowski, G.; Kubacka, M. Navigational Risk Assessment in Offshore Wind Farms Using Spatial Ship Domain Models. *Appl. Sci.* **2025**, *15*, 6943. [CrossRef]
5. Baekalov, I.; Bulian, G.; Cichowicz, J.; Eliopoulou, E.; Konovessis, D.; Leguen, J.-F.; Rosen, A.; Themelis, N. Ship Stability, Dynamics and Safety: Status and Perspectives from a Review of Recent STAB Conferences and ISSW Events. *Ocean. Eng.* **2016**, *116*, 312–349. [CrossRef]
6. Homsi, G.; Martinelli, R.; Vidal, T.; Fagerholt, K. Industrial and Tramp Ship Routing Problems: Closing the Gap for Real-Scale Instances. *Eur. J. Oper. Res.* **2020**, *283*, 972–990. [CrossRef]
7. dos Santos, P.T.G.; Kretschmann, E.; Borenstein, D.; Guedes, P.C. Cargo Routing and Scheduling Problem in Deep-Sea Transportation: Case Study from a Fertilizer Company. *Comput. Oper. Res.* **2020**, *119*, 104934. [CrossRef]
8. Wu, L.; Wang, S.; Laporte, G. The Robust Bulk Ship Routing Problem with Batched Cargo Selection. *Transp. Res. Part B Methodol.* **2021**, *143*, 124–159. [CrossRef]
9. Gao, Y.; Sun, Z. Tramp Ship Routing and Speed Optimization with Tidal Berth Time Windows. *Transp. Res. Part E Logist. Transp. Rev.* **2023**, *178*, 103268. [CrossRef]
10. He, P.; Jin, J.G.; Pan, W.; Chen, J. Route, Speed, and Bunkering Optimization for LNG-Fueled Tramp Ship with Alternative Bunkering Ports. *Ocean Eng.* **2024**, *305*, 117957. [CrossRef]
11. Omholt-Jensen, S.; Fagerholt, K.; Meisel, F. Fleet Repositioning in the Tramp Ship Routing and Scheduling Problem with Bunker Optimization: A Matheuristic Solution Approach. *Eur. J. Oper. Res.* **2025**, *321*, 88–106. [CrossRef]
12. Tamburini, A.; Lange, N.; Pisinger, D. A Rich Model for the Tramp Ship Routing and Scheduling Problem—Solved through Column Generation. *Transp. Res. Part E Logist. Transp. Rev.* **2025**, *198*, 104019. [CrossRef]
13. Eide, L.; Ardal, G.C.H.; Evsikova, N.; Hvattum, L.M.; Urrutia, S. Load-Dependent Speed Optimization in Maritime Inventory Routing. *Comput. Oper. Res.* **2020**, *123*, 105051. [CrossRef]
14. Ulsrud, K.P.; Vandvik, A.H.; Ormevik, A.B.; Fagerholt, K.; Meisel, F. A Time-Dependent Vessel Routing Problem with Speed Optimization. *Eur. J. Oper. Res.* **2022**, *303*, 891–907. [CrossRef]
15. Li, M.; Fagerholt, K.; Schütz, P. Stochastic Tramp Ship Routing with Speed Optimization: Analyzing the Impact of the Northern Sea Route on CO_2 Emissions. *Ann. Oper. Res.* **2025**, *350*, 299–323. [CrossRef]
16. Huang, X.; Liu, Y.; Sha, M.; Han, B.; Han, D.; Liu, H. ETE-SRSP: An Enhanced Optimization of Tramp Ship Routing and Scheduling. *J. Mar. Sci. Eng.* **2024**, *12*, 817. [CrossRef]
17. Cheng, L.; Xu, L.; Bai, X. Cargo Selection, Route Planning, and Speed Optimization in Tramp Shipping under Carbon Intensity Indicator (CII) Regulations. *Transp. Res. Part E Logist. Transp. Rev.* **2025**, *194*, 103948. [CrossRef]
18. Hua, R.; Yin, J.; Wang, S.; Han, Y.; Wang, X. Speed Optimization for Maximizing the Ship's Economic Benefits Considering the Carbon Intensity Indicator (CII). *Ocean Eng.* **2024**, *293*, 116712. [CrossRef]
19. Guo, Y.; Wang, Y.; Zhang, L.; Wu, L.; Chen, X. Towards Sustainable Shipping: A Learning-Aided Route-Speed Joint Optimization Considering Energy Efficiency and Punctual Arrival. *Transp. Res. Part E Logist. Transp. Rev.* **2026**, *205*, 104489. [CrossRef]
20. Golsefidi, M.M.; Sharifi, M.A.; Ghader, S. Containerships Routing Problem: Incorporating Uncertain Weather Impact on Fuel Consumption by Considering Speed Optimization. *Ocean Eng.* **2025**, *340*, 122410. [CrossRef]
21. Timas, A.; Mohammadi, M. Integrating Weather-Informed Routing and Energy Optimization for Sustainable Maritime Transportation. *Ocean Eng.* **2025**, *333*, 121463. [CrossRef]
22. Ok, M.; Lei, H. Accurate and Robust Linear Representation for Containership Stability Conditions with Ballast Water. *Ocean Eng.* **2024**, *306*, 118141. [CrossRef]
23. Wang, L.; Liao, S.; Wang, S.; Jia, B.; Yin, J.; Li, R. Real-Time Prediction of Metacentric Height of Ro-Ro Passenger Ships in Qiongzhou Strait Based on Improved RBF Neural Network. *Ocean Eng.* **2024**, *312*, 119067. [CrossRef]
24. Song, S.; Kim, D.; Dai, S. CFD Investigation into the Effect of GM Variations on Ship Manoeuvring Characteristics. *Ocean Eng.* **2024**, *291*, 116472. [CrossRef]
25. El Yaagoubi, A.; Charhbili, M.; Boukachour, J.; El Hilali Alaoui, A. Multi-Objective Optimization of the 3D Container Stowage Planning Problem in a Barge Convoy System. *Comput. Oper. Res.* **2022**, *144*, 105796. [CrossRef]
26. van Twiller, J.; Sivertsen, A.; Pacino, D.; Jensen, R.M. Literature survey on the container stowage planning problem. *Eur. J. Oper. Res.* **2024**, *317*, 841–857. [CrossRef]
27. Ling, Y.; Wang, Q.; Pan, L. Advancing Multi-Port Container Stowage Efficiency: A Novel DQN-LNS Algorithmic Solution. *Knowl.-Based Syst.* **2024**, *299*, 112074. [CrossRef]
28. Zheng, H.; Fan, X.; Tang, C. Integrated Optimization of Berth Allocation Problem with Berth Shifting Strategies and Ballast Water Management for Dry Bulk Ports. *Ocean Eng.* **2024**, *309*, 118430. [CrossRef]

29. Elidolu, G.; Sezer, S.I.; Akyuz, E.; Arslan, O.; Arslanoglu, Y. Operational Risk Assessment of Ballasting and De-Ballasting on-Board Tanker Ship under FMECA Extended Evidential Reasoning (ER) and Rule-Based Bayesian Network (RBN) Approach. *Reliab. Eng. Syst. Saf.* **2023**, *237*, 108975. [CrossRef]
30. Wang, X.; Li, S.; Liu, Q.; Liu, Z. Sequential Matching Optimization for Lifting Trajectory and Ballast Water Allocation of the Intelligent Revolving Floating Crane. *Ocean Eng.* **2022**, *266*, 113061. [CrossRef]
31. Guo, Z.; Cao, Z.; Wang, W.; Jiang, Y.; Xu, X.; Feng, P. An Integrated Model for Vessel Traffic and Deballasting Scheduling in Coal Export Terminals. *Transp. Res. Part E Logist. Transp. Rev.* **2021**, *152*, 102409. [CrossRef]

Disclaimer/Publisher's Note: The statements, opinions and data contained in all publications are solely those of the individual author(s) and contributor(s) and not of MDPI and/or the editor(s). MDPI and/or the editor(s) disclaim responsibility for any injury to people or property resulting from any ideas, methods, instructions or products referred to in the content.